EXPERIMENTAL CHARACTERIZATION OF THE AERODYNAMIC WAKE OF A HIGH-CLEARANCE SPRAYER WITH CHANGING OPERATING PARAMETERS

Ian W. P. Paulson[1,*], Justin Gerspacher[1], Benjamin J. Gagnon[2], Hubert Landry[2], Thomas M. Wolf[3], David Sumner[2], Donald J. Bergstrom[2]

[1] Prairie Agricultural Machinery Institute, Humboldt, Saskatchewan, Canada.
[2] Department of Mechanical Engineering, University of Saskatchewan, Saskatoon, Saskatchewan, Canada.
[3] Agrimetrix Research and Training, Saskatoon, Saskatchewan, Canada.
[*] Correspondence: ipaulson@pami.ca

HIGHLIGHTS

- Air velocity data were measured at seven lateral positions across the width of a modern high-clearance sprayer at multiple vertical and downstream locations relative to the nozzles. Velocity components were measured in three directions.
- Complex flow patterns were present behind the sprayer tractor and rear tires. An upward velocity component was measured below and downstream of the nozzles at many of the sensor locations.
- Elevated turbulent kinetic energy was measured downstream of the structural elements required for reconfiguring the boom structure into the transport position.

ABSTRACT. *With growing pressure for increased efficiency and productivity on large farms throughout North America, high-clearance sprayers have become large machines that are operated at relatively high speed when applying pesticides during the growing season. Minimizing pesticide drift remains paramount to the safe and responsible operation of these machines. With the aim of both improving the understanding of high-clearance sprayer wake features, and to aid in the validation of numerical models of a full-scale sprayer using computational fluid dynamics (CFD), time-averaged velocity components and turbulent kinetic energy (TKE) in the wake of a sprayer were measured and reported during simulated field operation. Data were collected at various locations in the wake of a sprayer at two operating speeds (4 and 11 m s^{-1}) at two boom heights. Ultrasonic anemometers were located directly behind the sprayer, immediately beside the sprayer tractor, and farther down the boom away from the influence of the tractor. Complex flow patterns were present behind the sprayer tractor and rear tires. An upward velocity component was measured below and downstream of the nozzles at many of the sensor locations. The magnitude of turbulence, upward velocity, and velocity deficit generally increased as the reference airspeed (travel speed combined with headwind contributions) increased. A lower boom height reduced the severity of these detrimental wake characteristics near the sprayer tractor; in general, a lower boom is known to reduce the potential of spray drift. Overall, this experimental study illustrates the variation in wake features behind a modern high-clearance sprayer under different operating conditions.*

Keywords. *High-clearance sprayer, Spray drift, Turbulent wake, Ultrasonic anemometer.*

Pesticide application remains a critical step in modern agricultural practices. On many broad-acre farms throughout North America, self-propelled high-clearance sprayers have become an important tool to achieve timely and efficient pesticide application. In this push for productivity, high-clearance sprayers have become large machines that operate at relatively high speed. A better understanding of their aerodynamic properties is required to maintain the high productivity of large sprayers while minimizing spray drift.

A significant body of literature has been developed through experimental work and numerical studies in investigating and predicting the risk of pesticide drift (Butler Ellis and Miller, 2010; Teske et al., 2002; Nuyttens et al., 2007); however, the effect of mechanisms related to the sprayer itself have often been neglected. As part of a larger effort to consider the aerodynamic effects of modern high-clearance design and operating choices, field experiments were conducted to characterize the wake in targeted regions behind a modern high-clearance sprayer while operating under a variety of real-world conditions. In addition to increasing the fundamental understanding of the wakes present near these large machines during their operation, the measured data will also be used for the ongoing development and validation of a numerical model using computational fluid dynamics (CFD).

Submitted for review on 3 November 2021 as manuscript number MS 14941; approved for publication as a Research Article by Associate Editor Dr. Harold Thistle and Community Editor Dr. Heping Zhu of the Machinery Systems Community of ASABE on 3 April 2022.

  ISSN 2769-3295 https://doi.org/10.13031/ja.14941

Landry and Wolf (2019) reported a methodology for measuring air velocity components behind a modern high-clearance sprayer while in operation using ultrasonic anemometers. Turbulent kinetic energy (TKE), a scalar turbulence metric, was found to vary significantly depending on the measurement location behind the sprayer. A similar measurement approach has been adopted in the present experimental study.

It was reported by Landry and Wolf (2019) that the presence of a liquid spray did not significantly affect the measured TKE. These results were in agreement with Teske et al. (2016a), who concluded that the velocity and turbulence fields measured downstream of a section of sprayer boom in a wind tunnel were unaffected by the introduction of spray. Although the larger goal of the present work is to study the effect of the sprayer wake on droplet trajectories using CFD, the need for a representative sprayer wake in a CFD model, initially without droplets, is imperative. It should be noted, however, that sheet blockage effects due to the presence of sprayer nozzle effluent closer to spray nozzles have been documented (Murphy et al., 2000).

Teske et al. (2016b) characterized the downstream flow field with a simulated headwind approaching from several directions using a stationary scale model (1:25) of a sprayer in a wind tunnel. Detailed component-wise data from a headwind-only scale model test were also reported (Teske et al., 2015). The presence of the boom and tractor in the airflow patterns of the wind tunnel was evident from the complex wake downstream of the sprayer. Disturbances at the outboard articulating joints on the boom were also noted. In the present study, conducted in the field using an actual sprayer, these regions were specifically examined.

Materials and Methods

Initial work by Landry and Wolf (2019) explored the suitability of ultrasonic anemometers (model 81000, R.M. Young Co.) for use in wake characterization. A similar approach with similar instrumentation was adopted for the field experiments in the present study. Details of the test machinery, instrumentation, and data reduction procedure are outlined below.

Sprayer and Instrumentation

A John Deere 4830 self-propelled high-clearance sprayer, shown in figure 1, was used for the field experiments. This model was produced between approximately 2007 and 2014, with many units actively in use on farms across North America. The field experiments were conducted over two autumn periods: 12, 13, and 18 October 2019, and 7, 9, and 16 October 2020. A nominally flat test field near Saskatoon, Saskatchewan, Canada, was selected. Weather conditions are reported in the Results and Discussion section.

The height of the sprayer was 3.87 m, and the tire track width (tire center to center) was 3.04 m. The sprayer was fitted with 320/90R50 tires. At the first vertical support of the boom structure outside of the rear tire, the boom structure was approximately 0.72 m tall; the outer boom section was approximately 0.36 m tall.

An adjustable aluminum frame was used to support three ultrasonic anemometers on the sprayer boom in various positions relative to the nozzles. Three regions of interest were explored during this work: far along the boom (Far Boom), immediately behind and outside of the rear tire (Near Boom), and directly behind the sprayer tractor (Behind Tractor). The aluminum frame, mounted for measurements in the Behind Tractor region, is shown in figure 2. The adjustable frame and anemometers were leveled when the measurement location was changed; the alignment error of the anemometers from true vertical orientation during setup was estimated to be ±2°. This source of uncertainty is not reflected in the error quantifications provided in the Results. Additionally, when the anemometers were fixed to the boom structure, their orientation relative to level ground changed with the orientation of the boom during operation; this change in orientation was not measured. Selecting a flat, level field helped to minimize this source of error, but it was not corrected for in the analysis.

In the Far Boom configuration, the three anemometers were located 8.30, 6.63, and 4.97 m laterally (along the boom) from the centerline of the sprayer. In the Near Boom configuration, the lateral positions were 4.97, 2.89, and 1.52 m. Finally, when measuring behind the tractor, the anemometers were 1.52 m to the left of center, on the centerline of the sprayer, and 0.92 m to the right of center. Therefore, the sensors overlapped at the lateral positions behind the tractor tire (1.52 m) and between the Near Boom and Far

Figure 1. John Deere 4830 high-clearance sprayer used in field experiments.

Figure 2. Aluminum frame used to mount three anemometers on the boom, shown in the Behind Tractor configuration. The anemometers were oriented upside down in this measurement region.

Boom positions (4.97 m). Data from the Near Boom configuration were collected in 2019. The Far Boom and Behind Tractor configurations were tested in 2020.

Due to time and geometric limitations, a full-factorial combination of all measurement positions behind the nozzle with all elevations relative to the nozzle was not completed. The specific locations of the anemometers relative to the nozzles are given in table 1, including the position numbers used in subsequent statistical analyses.

Some geometric asymmetry was present due to the presence of the operator's platform and flip-up access ladder on the left side of the machine; however, the large structural features (engine compartment, cab, product tank, and boom components) were symmetrical about the centerline of the sprayer.

Three coordinate systems were considered as part of the analysis. The ambient wind conditions were measured with a stationary weather station in a fixed frame, with 0° aligned with compass north (east and west are +90° and -90°, respectively). A local coordinate system, coincident with the sprayer, was used to report all measured data. Convention within fluid mechanics has positive air velocity vectors oriented in the direction of the airflow (as opposed to a typical meteorological convention that reports the direction from which wind is blowing), so +*x* of the sprayer coordinate system was aligned opposite the direction of travel of the sprayer, i.e., a motion-induced headwind was a positive quantity as air traveled backward relative to the sprayer. To maintain +*z* in the sprayer coordinate system pointing upward, the +*y* axis pointed toward the end of the right sprayer boom (when facing forward). Finally, the coordinate system within which the anemometer measurements were reported had to be considered because, as shown in figure 2, the orientation of the anemometers changed depending on the measurement location.

The instrumentation and data acquisition equipment used during the field experiments are listed in table 2. The ultrasonic anemometer data acquisition rate was set to 4 Hz during the 2019 field experiments and 32 Hz (hardware maximum) during the 2020 field experiments. The weather station recorded conditions at 1 Hz.

During the 2019 field experiments, data were collected while running both north and south on a common track to create headwind or tailwind conditions relative to the sprayer. The orientation of the measurement runs in 2020 was east and west, again to create headwind or tailwind conditions.

Data Reduction

Operating parameters for the three measurement regions are detailed in table 3. Four replications of each treatment were performed in each direction of travel. Individual data files were generated from each measurement run. The start and end of steady-state tractor speed and heading were manually identified from each file; data outside this period were discarded from the analysis. At the fastest travel speed, at least 15 s of steady-state data were collected per measurement run.

All anemometer measurements were checked for errant measurement samples that occasionally occurred due to the high concentration of dust that was present during some of the measurement runs at some sensor locations. These samples were obvious in the anemometer data, as transducer output saturated at the maximum value for several samples before returning to a normal output. For measurement runs in which the concentration of errant measurements in an anemometer time history exceeded 1.5% of all samples, those runs were excluded from further analysis. This most often occurred when the anemometer was directly behind and in close proximity to the rear tire. If the concentration of errant measurements did not exceed 1.5%, the errant samples and two samples before and after the errant spike were removed from the subsequent calculations.

Measured velocity data were converted from the reported speed (magnitude)-heading-elevation components to *u*-*v*-*w* components relative to the sprayer coordinate system using the following transformations when the anemometers were oriented in the standard cage-up orientation:

$$u(t) = V_{Mag}(t) * \cos\theta_{Elev}(t) * \cos\left(360° - \phi_{Heading}(t)\right) \quad (1)$$

$$v(t) = V_{Mag}(t) * \cos\theta_{Elev}(t) * \sin\left(360° - \phi_{Heading}(t)\right) \quad (2)$$

$$w(t) = V_{Mag}(t) * \sin\left(\theta_{Elev}(t)\right) \quad (3)$$

Table 1. Elevation (relative to nozzles), distance behind nozzles, and lateral distance from tractor centerline of the three anemometers in the three measurement regions.

Measurement Region	Relative Elevation	Distance Behind Nozzle (m) [*Position number*]	Lateral Position Left of Sprayer Centerline (m)
Near Boom	In nozzle plane	0.43, 0.79, 1.42	4.97, 2.89, 1.52
Far Boom	In nozzle plane	0.43 [*1*], 0.79 [*2*]	8.30, 6.63, 4.97
	0.2 m below nozzle plane	0.0 [*3*], 0.43 [*4*], 0.79 [*5*], 1.42 [*6*]	-
Behind Tractor	1.02 m above nozzle plane	0.79 [*1*], 1.42 [*2*]	-0.92 (right of center), 0.0, 1.52
	In nozzle plane	0.43 [*3*], 0.79 [*4*], 1.42 [*5*]	-
	0.2 m below nozzle plane	0.43 [*6*], 0.79 [*7*]	-

Table 2. Instruments and data acquisition system used during the field experiments.

Description	Make	Model	Resolution	Range	Accuracy
Ultrasonic anemometers	Young	81000	0.01 m s^{-1} and 0.1°	0 to 40 m s^{-1}, 0° to 360° azimuth, ±60° elevation	±1% RMS ±0.05 m s^{-1}, ±2°
Weather station	Onset Hobo	H21-002	0.02°C at 25°C, 0.1% RH	-40°C to 75°C, 0% to 100% RH	±0.21°C, ±2.5% from 10% to 90% RH
Wind speed and gust measurement	Onset	S-WSB-M003	0.5 m s^{-1}	0-76 m s^{-1}	±1.1 m s^{-1}, 1.0 m s^{-1} starting threshold
Wind direction	Onset	S-WDA-M003	1.4°	0° to 355°	±5°, 1.0 m s^{-1} starting threshold
Data acquisition system	Somat	eDAQ (ECPU, ECOM, EHLS)	16 bit	-	-
GPS receiver	Garmin	GPS18x-5Hz	-	0-515 m s^{-1}	0.05 m s^{-1}

Table 3. Operating parameters during data collection in the three measurement regions.

Parameter	Near Boom	Behind Tractor	Far Boom
Speed (m s^{-1})	4, 11	4, 11	4, 11
Nozzle height (m)	0.64, 1.14	0.64, 1.14	1.63, 1.14[a]
Travel direction	North, south	East, west	East, west
Anemometer height relative to nozzle (m)[b]	-0.2, 0.0	-0.2, 0, 1.02	-0.2, 0.0
Anemometer location behind nozzle (m)[b]	0.43, 0.79, 1.42	0.43, 0.79, 1.42	0.0, 0.43, 0.79, 1.42

[a] Only measurements with sensors positioned at 0.0 m behind and 0.2 m below the nozzles were recorded with a boom height of 1.63 m.
[b] A full-factorial matrix of all combinations of anemometer relative height and location was not performed. See table 1 for specific locations.

where $u(t)$, $v(t)$, and $w(t)$ are the time-varying components of velocity in the x, y, and z directions, respectively; $V_{Mag}(t)$ is the velocity magnitude; $\theta_{Elev}(t)$ is the elevation angle of the airflow; and $\phi_{Heading}(t)$ is the heading angle of the airflow.

For treatments in which the anemometers were oriented in a nonstandard cage-down orientation, the heading angle argument ($360° - \phi_{Heading}$) in equations 1 and 2 simplified to ($\phi_{Heading}$), and a factor of -1 was applied to equation 3.

A time-varying velocity, $u(t)$, can be defined as the sum of a time-average component $\overline{u}$ and a time-varying component $u(t)'$ as:

$$u(t) = \overline{u} + u(t)' \tag{4}$$

Both components are of interest. The time-varying component is related to the turbulence of the airflow. Turbulent kinetic energy (TKE) is a scalar measure of turbulence. It is defined by:

$$\text{TKE} = 0.5\left(\overline{u'^2} + \overline{v'^2} + \overline{w'^2}\right) \tag{5}$$

where $\overline{u'^2}$, $\overline{v'^2}$, and $\overline{w'^2}$ are the variances of measured air velocity in the x, y, and z directions. The mean components of the velocity ($\overline{u}$, $\overline{v}$, and $\overline{w}$) are the simple arithmetic means of the steady-state period of the measured data.

The ambient wind speed and direction were recorded using a separate weather station. The period of the measurement run was identified in the weather file with an additional 30 s buffer at the start and end of the measurement period included in the calculation of per-run ambient wind speed and direction. The transformation of wind data from the fixed N-E coordinate system to the on-sprayer coordinate system is given by:

$$\varphi_{wind/SCS} = 360° - \varphi_{wind/heading} \tag{6}$$

where $\varphi_{wind/SCS}$ is the wind direction with respect to the sprayer coordinate system where positive $+x$ points rearward on the sprayer, and $\varphi_{wind/heading}$ is the direction of the wind with respect to the heading of the sprayer.

An average reference airspeed (U_{ref}), reflecting both the travel speed and the contribution of ambient wind speed of each measurement, was calculated as:

$$U_{ref} = \overline{u}_{GPS} + \overline{u}_{wind/sprayer} \tag{7}$$

where $\overline{u}_{GPS}$ is the time-averaged travel speed of the sprayer measured using GPS, and $\overline{u}_{wind/sprayer}$ is the u component of ambient wind velocity with respect to the sprayer.

File handling, calculations, and data reduction and visualization were conducted using Python (Python, 2021). The statistical calculations were performed using Minitab 18 (Minitab, 2019).

RESULTS AND DISCUSSION

Ambient wind data are reported first to provide context to the weather conditions present during field testing. To characterize the flow patterns around a high-clearance sprayer in the context of consistent pesticide delivery, the mean velocity components of airflow and turbulence were both of interest, as the trajectory of spray droplets is potentially affected by both. Average streamwise velocity deficit values are reported and discussed, followed by the mean values of v and w components. Finally, turbulent kinetic energy is presented and discussed.

WEATHER CONDITIONS

The ambient wind speed and direction during the testing days in 2019 and 2020 are plotted in figure 3. Wind conditions were very calm in 2019 with the ambient wind speed during much of the testing period below 2 m s^{-1}. Anemometer stall was not investigated directly, but the very calm conditions on 13 and 18 October 2019 were verified against historical weather data from Environment Canada (2019) recorded at the local airport (YXE) approximately 4 km away.

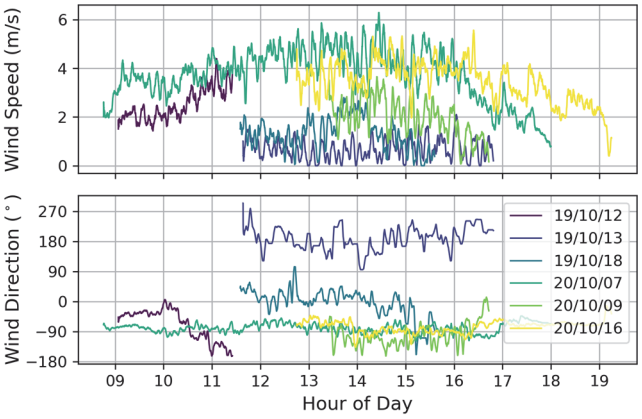

Figure 3. Ambient wind data during testing days in 2019 and 2020.

The maximum hourly average windspeed at a height of 10 m during the testing period was less than 1.5 m s^{-1}. Therefore, while stall may have been present in portions of the data, the true ambient wind speed was very low. In comparison, the ambient wind speed in 2020 was greater but better represented conditions in which spraying would typically occur. The wind was consistently from the west during the 2020 tests; the sprayer was driven along an east-west oriented path in both directions during testing.

Longitudinal Velocity

In this section, the measurements of the longitudinal (streamwise) component of velocity (u) at each sensor location for the three regions of interest are discussed; ambient headwind and tailwind data are also reported. The effect of the ambient headwind is discussed, as the total streamwise velocity with respect to the sprayer is important to consider when assessing the wake characteristics of the machine.

Near Boom

The average reference airspeed, defined by equation 7, for each combination of measurement position, travel speed, and direction, are presented in table 4. Given the calm testing conditions present during data collection in 2019, the difference between ground speed and reference airspeed was typically less than 1 m s^{-1}. The greatest directionality effect was present at 11 m s^{-1} in the high boom position (where nozzles were 1.14 m above the ground) when measuring at the maximum distance behind the nozzles (1.42 m). Note that the three ultrasonic anemometers, in their respective lateral locations, were recorded simultaneously per run, so a reference airspeed value applies to a given run and not to an individual lateral sensor position.

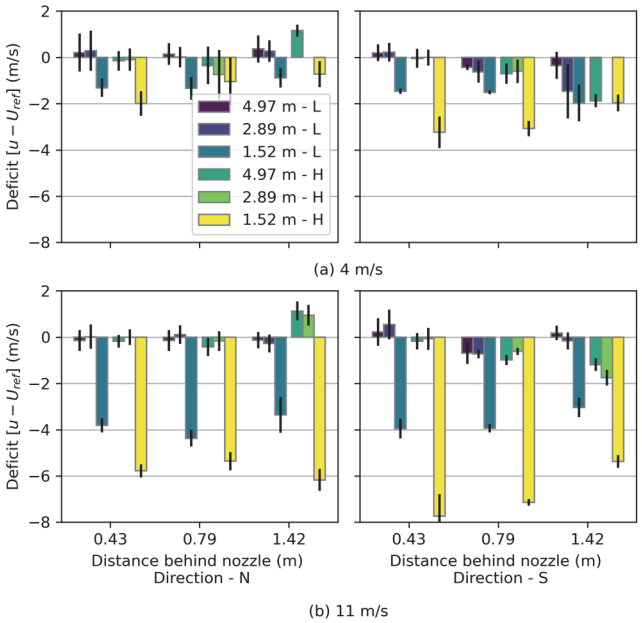

Figure 4. Mean velocity deficits measured in the Near Boom region in the nozzle plane at two nozzle heights (L = 0.64 m, and H = 1.14 m), and at 0.43, 0.79, and 1.42 m behind the nozzles while traveling north (tailwind; left column) and south (headwind; right column) at travel speeds of (a) 4 m s^{-1} and (b) 11 m s^{-1}. Error bars represent standard deviations of the runs included in the mean.

Ambient wind speed is effectively additive to the sprayer ground speed. The effect of varying reference airspeed was subtracted from the measured longitudinal velocity to create the relative metric of velocity deficit ($u - U_{ref}$). A negative value indicates that the local measured airspeed was less than the reference airspeed. Values near 0 indicated that the measured airspeed was similar to the reference value, and a positive velocity deficit indicated that local airflow had accelerated relative to the reference value.

Velocity deficit data at travel speeds of 4 and 11 m s^{-1}, for the Near Boom region, are presented in figure 4. The largest velocity deficit was present directly behind the left rear tractor tire at the lateral location of 1.52 m. This deficit was larger when the boom was at the higher position (static nozzle height of 1.14 m above the ground). For a given travel speed, the effect of height on velocity deficit at this sensor location was greater when traveling south, likely due to the contribution of headwind to reference airspeed. Farther outward of the tractor tire, the velocity deficit was well below 1 m s^{-1} in most cases, with seemingly little influence from travel speed.

Table 4. Means and standard deviations of the reference airspeeds measured during runs of each treatment combination, when measuring in the Near Boom region.

Travel Speed (m s^{-1})	Direction	Boom Height (m)	Reference Airspeed (m s^{-1})					
			0.43 m Behind Nozzle		0.79 m Behind Nozzle		1.42 m Behind Nozzle	
			Mean	SD	Mean	SD	Mean	SD
4	North	0.64	3.56	0.50	3.69	0.38	4.27	1.45
		1.14	3.74	0.56	2.98	0.72	5.58	0.23
	South	0.64	4.54	0.54	4.28	0.25	4.38	0.81
		1.14	4.70	0.60	4.81	0.42	3.17	0.33
11	North	0.64	10.71	0.25	10.31	0.57	10.41	0.35
		1.14	10.34	0.39	9.96	0.58	12.34	0.24
	South	0.64	11.21	0.21	11.63	0.21	11.76	0.11
		1.14	11.91	0.48	11.80	0.15	9.70	0.34

Far Boom

The average reference airspeeds during measurements in the Far Boom region are plotted in table 5. For a given combination of travel speed, direction, and height relative to the nozzles, the reference airspeeds remained consistent except when traveling west at 11 m s^{-1} when measuring below the nozzles. A trend of decreasing wind contribution as the measurement position moved farther behind the boom is evident due to the changing ambient wind speed throughout the day. The wind was from the west, so ambient wind added to the ground speed when traveling west and reduced the reference airspeed when traveling east.

The velocity deficits measured in the Far Boom region at 4 and 11 m s^{-1} travel speeds are presented in figure 5. At both speeds, a deficit existed in the nozzle plane; the deficit was speed-dependent and present in both travel directions. This differed from the apparent lack of deficit and speed dependency measured in the Near Boom region. The average magnitude of the velocity deficit in the Far Boom region was greater than the deficit at the sensors located at 4.97 and 2.89 m when measuring in the Near Boom region. Because the left-most Near Boom anemometer and the right-most Far Boom anemometer were in the same location (4.97 m), closer agreement was expected. The differences are likely attributable to ambient wind condition effects, particularly the presence of a slight *v* component of ambient wind (with respect to the sprayer coordinate system) during the 2020 data collection period; this may also highlight an effect of the tractor in the Near Boom results.

Below the nozzle plane at 4 m s^{-1}, the effect of the boom was small, and the sign of the deficit appeared to be direction-dependent. Positive values indicate flow acceleration at the measurement location, which occurred when traveling west at both travel speeds. However, at 11 m s^{-1}, the deficit was negligible below and farther behind the nozzles in both directions.

Overall, the velocity deficit appeared to be greater in the nozzle plane than below the nozzles; this was confirmed using a two-sample t-test (Minitab, 2019) between measurements grouped by their position, i.e., in the nozzle plane (sensor positions 1 and 2, see table 1) and below the nozzle plane (sensor positions 3 through 6). In the nozzle plane, the mean velocity deficit was -2.28 m s^{-1}, compared to a mean value of 0.271 m s^{-1} below the nozzle plane. Consequently, the data were split into two subsets for further analysis. The explicit split was performed due to the presence of both positive and negative velocity deficit values included in the group means.

After grouping the data, separate Johnson transformations were applied to each dataset to adjust for a lack of normality. Minitab (2019) automatically selects the type of Johnson transformation (type SU, SB, or SL) based on the method described by Chou et al. (1998). A general linear model was developed using speed, direction, lateral sensor

Table 5. Means and standard deviations of reference airspeeds measured during runs of each treatment combination in Far Boom region.

Travel Speed (m s^{-1})	Travel Direction	Sensor Height	Reference Airspeed (m s^{-1}) at Different Sensor Distances							
			0 m Behind Nozzle		0.43 m Behind Nozzle		0.79 m Behind Nozzle		1.42 m Behind Nozzle	
			Mean	SD	Mean	SD	Mean	SD	Mean	SD
4	East	In nozzle plane	-	-	1.88	0.22	2.24	0.17	-	-
		0.20 m below	1.31	0.29	1.16	0.64	1.20	0.68	1.93	0.38
	West	In nozzle plane	-	-	6.58	0.19	6.56	0.13	-	-
		0.20 m below	7.96	0.94	8.15	0.62	7.86	0.64	7.65	0.27
11	East	In nozzle plane	-	-	9.22	0.25	8.79	0.44	-	-
		0.20 m below	7.37	0.22	7.85	0.25	7.90	0.53	8.58	0.20
	West	In nozzle plane	-	-	13.26	0.13	13.24	0.42	-	-
		0.20 m below	15.36	0.56	14.67	0.15	13.79	0.21	13.92	0.17

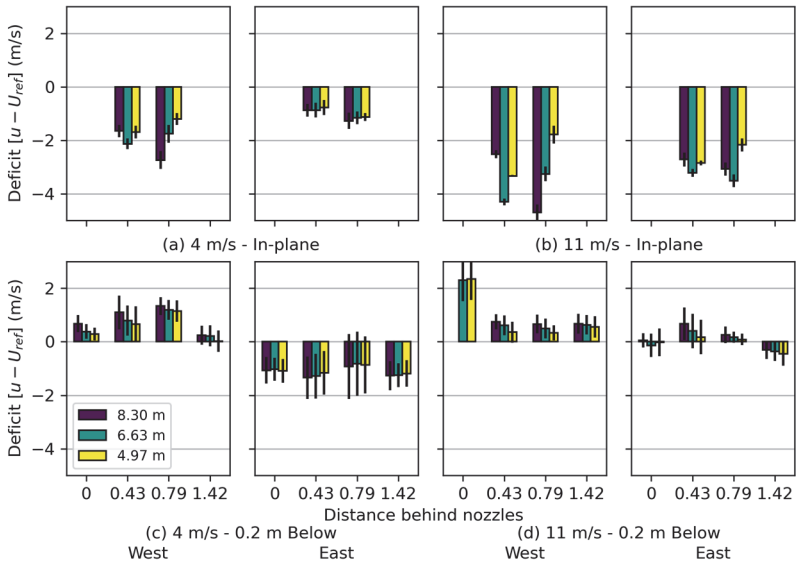

Figure 5. Mean velocity deficits measured in the Far Boom region while traveling (a and c) 4 m s^{-1} and (b and d) 11 m s^{-1} in plane with the nozzles (a and b) and 0.2 m below the nozzles (c and d) at three lateral locations (8.30, 6.63, and 4.97 m) while traveling west and east (headwind and tailwind, respectively). Error bars represent standard deviations of the runs included in the mean.

location, and the position of the sensor relative to the distance behind the nozzle (relative elevation was removed from consideration by the creation of the data subsets). A comparison of means for each subset is presented in table 6.

In this region of interest far down the boom, the lateral location along the boom only contributed a significant difference to the velocity field in the nozzle plane. In contrast to the air velocity measured along the boom near the tractor, when farther away from the tractor the effect of the tractor wake was less pronounced.

Velocity deficit, a quantity that is inherently relative to the freestream flow conditions, should be insensitive in a first-order sense. While speed was significant in both data subsets, the significance of direction on velocity deficit indicated that the size of the wake behind the boom away from the tractor was either nonlinearly related to the freestream flow conditions or was influenced by crosswind (which alternated direction with respect to the sprayer as the travel direction changed). Except for position 6 (farthest downstream of the boom), the position behind the boom was insignificant to the Far Boom velocity deficit measurements.

Table 6. Comparison of mean velocity deficits in the Far Boom region grouped into measurements in the nozzle plane and below the nozzles for the experimental treatments. Each group had a separate Johnson transformation applied to correct normality. Means with different letters under each treatment within each subgroup are significantly different according to Tukey's pairwise comparison tests at a 95% confidence level.

	In Nozzle Plane		Below Nozzles	
Treatment	Mean-Johnson (SB)	Grouping	Mean-Johnson (SU)	Grouping
Travel speed (m s^{-1})				
4	0.684	a	-0.282	a
11	-0.690	b	0.217	b
Travel direction				
West	-0.306	a	0.578	a
East	0.300	b	-0.643	b
Lateral sensor location (m)				
8.30	-0.158	a	0.072	a
6.63	-0.181	a	-0.027	a
4.97	0.330	b	-0.143	a
Position number				
1	0.055	a	-	
2	-0.061	a	-	
3	-		0.116	a
4	-		0.096	a
5	-		0.201	a
6	-		-0.543	b

Behind Tractor

The average reference airspeeds for each combination of measurement position, travel speed, boom height, and direction are shown in table 7. The velocity deficits measured for the Behind Tractor region are reported in figure 6. In comparison to the velocity deficits reported in the Far Boom region, the magnitude of the deficit behind the tractor was greater, particularly 1.02 m above the nozzles. The flow acceleration evident below and closely behind the nozzles in the Far Boom region was not present behind the tractor; instead, a velocity deficit was present. However, the deficit was greater in the nozzle plane compared to below the nozzles. This difference was also observed by Teske et al. (2015).

The deficit at the centerline sensor (0.0 m) when located above the nozzles was large and independent of travel speed and direction. Further inspection of the raw measured airflow data revealed reversed flow at this location during most tests. Reversed flow was not observed at similar measurement locations in the wind tunnel tests (Teske et al., 2015); however, the streamwise component reported in that study was as small as 5% of the freestream value at a similar elevation as the low boom and 1.02 m above the nozzle position measured in this work.

Because of the difference in flow field experienced by the anemometers when above the nozzles (in the shadow of the

Table 7. Means and standard deviations of the reference airspeeds measured during runs of each treatment combination, when measuring in the Behind Tractor region.

				Reference Airspeed (m s^{-1}) at Different Sensor Distances					
Travel Speed	Travel	Boom Height	Sensor	0.43 m Behind Nozzle		0.79 m Behind Nozzle		1.42 m Behind Nozzle	
(m s^{-1})	Direction	(m)	Height	Mean	SD	Mean	SD	Mean	SD
4	East	0.64	1.02 m above	-	-	2.44	0.07	1.49	1.19
			In nozzle plane	7.92	0.89	0.93	0.13	1.05	0.73
			0.2 m below	0.64	0.46	2.86	0.11	-	-
		1.14	1.02 m above	-	-	2.20	0.13	2.32	0.16
			In nozzle plane	1.45	0.31	1.18	0.69	1.16	0.92
			0.2 m below	1.16	0.27	3.41	0.20	-	-
	West	0.64	1.02 m above	-	-	5.99	0.73	7.68	0.53
			In nozzle plane	1.62	0.47	8.19	0.57	8.06	0.43
			0.2 m below	8.86	0.47	5.74	0.13	-	-
		1.14	1.02 m above	-	-	6.44	0.09	6.64	0.29
			In nozzle plane	8.22	1.17	8.11	0.89	7.69	0.45
			0.2 m below	7.63	1.85	5.15	0.22	-	-
11	East	0.64	1.02 m above	-	-	9.68	0.94	9.33	1.07
			In nozzle plane	10.97	0.31	10.59	0.53	9.74	0.42
			0.2 m below	9.20	0.62	9.30	0.81	-	-
		1.14	1.02 m above	-	-	9.45	0.26	9.95	0.63
			In nozzle plane	11.87	0.42	10.78	0.45	10.00	0.52
			0.2 m below	9.36	0.64	8.72	1.09	-	-
	West	0.64	1.02 m above	-	-	12.37	1.03	13.01	0.90
			In nozzle plane	11.61	0.13	12.02	0.58	12.74	0.37
			0.2 m below	12.76	0.53	13.36	1.15	-	-
		1.14	1.02 m above	-	-	13.05	0.22	12.65	0.53
			In nozzle plane	10.94	0.45	11.73	0.26	12.50	0.63
			0.2 m below	13.23	0.76	13.89	0.31	-	-

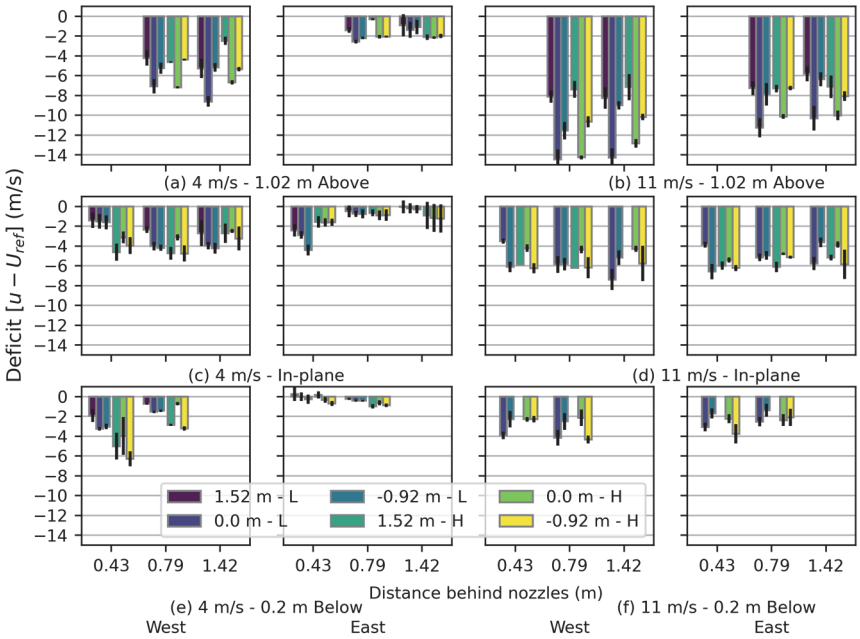

Figure 6. Mean streamwise velocity deficit ($u - U_{ref}$) for the Behind Tractor region at (a, c, e) 4 m s^{-1} and (b, d, f) 11 m s^{-1} and at two boom heights (L = 0.64 m and H = 1.14 m). Sensors were located 1.02 m above the nozzle plane (a and b), in the nozzle plane (c and d), and 0.2 m below the nozzle plane (e and f) at 0.43, 0.79, and 1.42 m behind the nozzles at three lateral positions (1.52, 0.0, and -0.92 m) while traveling west (headwind) and east (tailwind). Error bars represent standard deviations of the runs included in the mean.

frame and tank structure), compared to in the nozzle plane and below the nozzles (below the tractor frame), the dataset was split into those two subsets: positions 1 and 2, and positions 3 through 7 (see table 1 for sensor position numbers relative to the nozzles). To further identify factors that contributed to velocity deficit, normality of the subsets was verified, and a general linear model was fit using speed, direction, boom height, lateral sensor location, and sensor position relative to the nozzle. A comparison of means from both subsets is presented in table 8.

Table 8. Comparison of mean velocity deficits 1.02 m above nozzles and in the nozzle plane and 0.2 m below nozzles behind the tractor for the experimental treatments. Means with different letters under each treatment within each subgroup are significantly different according to Tukey's pairwise comparison tests at a 95% confidence level.

	1.02 m Above Nozzles		In Plane and 0.2 m Below Nozzles	
Treatment	Mean	Grouping	Mean	Grouping
Travel speed (m s^{-1})				
4	-3.560	a	-1.999	a
11	-9.449	b	-4.313	b
Travel direction				
West	-8.095	a	-3.859	a
East	-4.954	b	-2.452	b
Lateral sensor location (m)				
1.52	-4.980	a	-3.138	ab
0.0	-8.450	b	-2.946	a
-0.92	-6.144	c	-3.384	b
Position number				
1	-6.695	a	-	
2	-6.353	a	-	
3	-		-3.942	a
4	-		-3.807	a
5	-		-3.495	a
6	-		-2.526	b
7	-		-2.009	b
Boom height (m)				
0.64	-6.399	a	-2.960	a
1.14	-6.650	a	-3.352	a

Similar to the velocity deficit measured in the Far Boom region, travel speed and direction were significant factors influencing the velocity deficit in the Behind Tractor region in both subsets.

When measuring above the nozzles, lateral sensor location was found to be a significant factor, but boom height and the distance behind the boom were not found to be significant. This suggested a wake with some variation across the width of the machine (in a pairwise comparison, the mean of the sensor laterally located at 1.52 m was significantly different from the means of sensors laterally located at 0.0 and -0.92 m), with a recirculation zone along the central vertical plane of the tractor with an approximate height of at least 0.5 m and length of at least 0.6 m.

Mean Direction of Airflow

The average components of air velocity normal to the direction of travel (velocity components v and w) were computed to gain an understanding of the mean direction of airflow. Data from the three measurement regions of interest are discussed. In the vector plots, the v and w components are the average values from the runs at the measurement locations indicated; the vector tail coordinates indicate the measurement location on the sprayer. The red vector pair indicates a 1 m s^{-1} magnitude in both directions (grid squares represent 2.0 m s^{-1}). The shaded area around each arrow tip indicates ±1 σ of the values included in the average for each vector component. The horizontal blue arrows represent the average lateral ambient wind velocity relative to the tractor.

Near Boom

The vertical and lateral components of air velocity behind the boom near to the tractor are presented in figure 7. For brevity, only results at 11 m s^{-1} are presented. As a reminder,

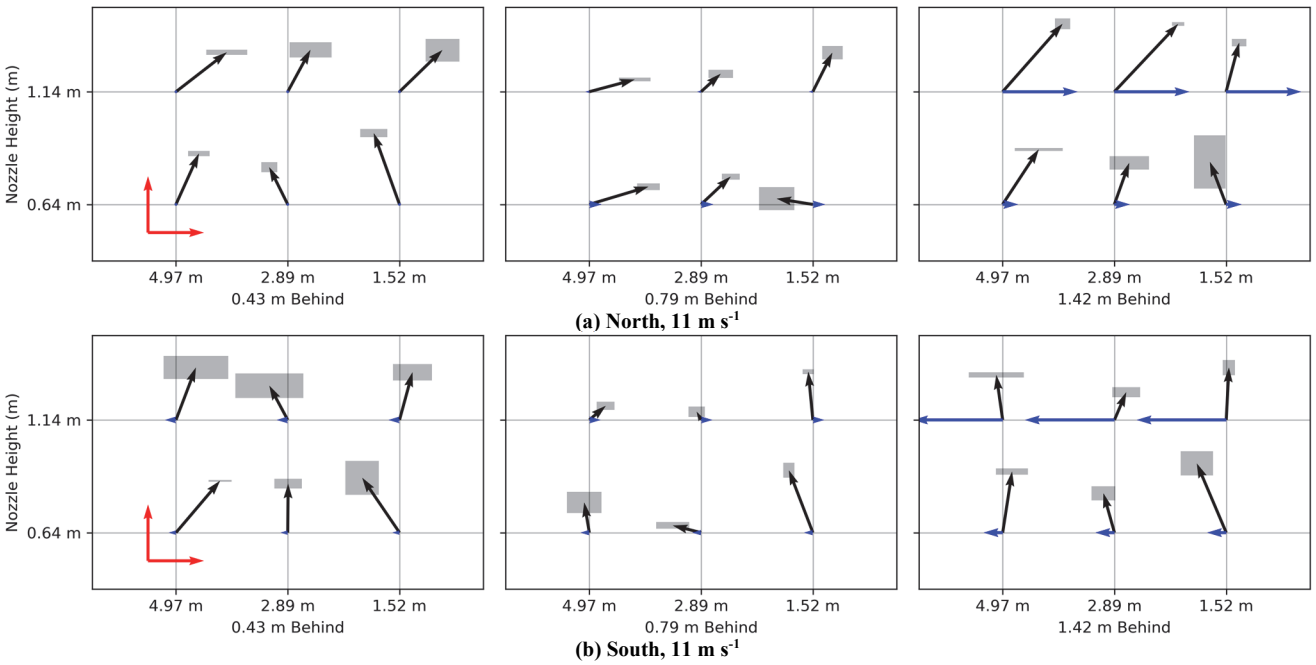

Figure 7. Near Boom multi-run average air velocity vectors (*v* and *w* components) measured at a ground speed of 11 m s^{-1} in a plane normal to the direction of travel: (a) north and (b) south.

a tailwind was present when traveling north; a headwind occurred when traveling south.

The *w* component of velocity was generally upward everywhere in the measured flow field. While the intended trajectory of droplets was downward from the sprayer, the flow field at the nozzle elevation downstream of the nozzles had a consistent upward velocity component. The sensitivity of airflow patterns to specific geometric features of the sprayer was not evaluated as part of this work; however, deposition performance would gain from minimizing these types of detrimental flow features during the design phase of future equipment. Upward velocity was consistently present behind the tire (lateral position of 1.52 m). At the lower boom height, an outward component was also consistently present behind the tire. Upwash behind a stationary wheel was observed in wind tunnel data (Teske et al., 2016b); strong spatial gradients in TKE were predicted in CFD models (Landry and Wolf, 2019), suggesting complex flow patterns immediately behind the tires.

The magnitude of the *w* component of velocity increased with reference airspeed (data from 4 m s^{-1} not shown). The *w* component values were corrected for normality using a Johnson transformation (type SB), and a general linear model was developed based on speed, direction of travel, nozzle height, distance behind the nozzles, and lateral sensor position. A comparison of means is presented in table 9.

Because the data were not normalized by the freestream velocity, the significance of travel speed and direction of travel were expected. The direction of travel was not significant; however, the ambient wind speed was very low during the Near Boom measurement period. Significant variations in the upward velocity component were found with changes both in lateral location and distance behind the nozzles. In the Near Boom region, the upward velocity component was not significantly affected by nozzle height.

Table 9. Comparison of mean *w* components of air velocity, after Johnson transformation (type SB), in the Near Boom region for the experimental treatments. Means with different letters under each treatment are significantly different according to Tukey's pairwise comparison tests at a 95% confidence level.

Treatment	Mean-Johnson	Grouping
Travel speed (m s^{-1})		
4	-0.702	a
11	0.560	b
Travel direction		
North	-0.112	a
South	-0.030	a
Lateral sensor location (m)		
4.97	0.093	a
2.89	-0.364	b
1.52	0.057	a
Distance behind nozzles (m)		
0.43	0.186	a
0.79	-0.641	b
1.42	0.241	a
Boom height (m)		
0.64	-0.048	a
1.14	-0.094	a

Far Boom

The mean vertical and lateral components of airflow in the Far Boom region are presented in figure 8, along with the average lateral component of ambient wind relative to the sprayer. For brevity, only results at 11 m s^{-1} are presented. The magnitudes of measured values when traveling east (with the wind) at 4 m s^{-1} were generally low, so interpretation of those data was uncertain. The general trends from the westbound data were similar between the 4 m s^{-1} and 11 m s^{-1} datasets.

Specific to the dataset for the Far Boom region, it was noted that the *w* component of airflow immediately below the nozzles was consistently negative when traveling at 11 m s^{-1}. In all other locations, the *w* component of velocity was upward everywhere in the measured flow field, similar

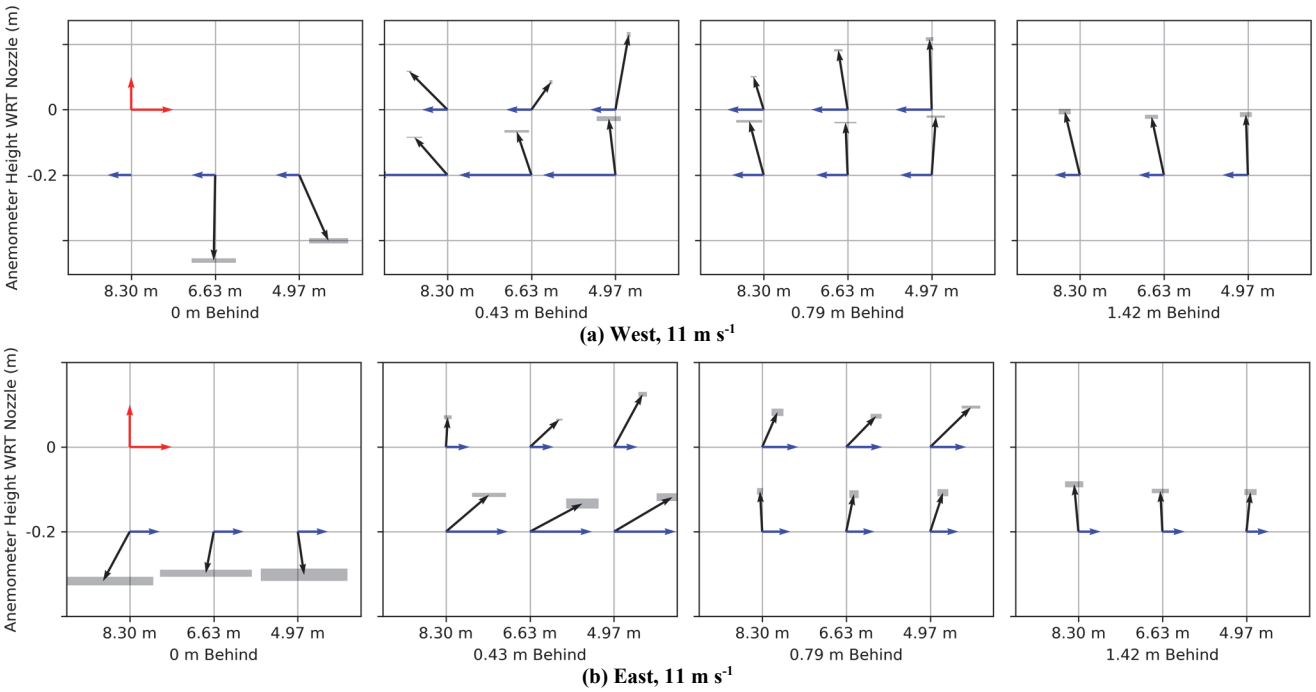

Figure 8. Far Boom multi-run average air velocity vectors (*v* and *w* components) measured at a ground speed of 11 m s^{-1} in a plane normal to the direction of travel: (a) west and (b) east.

to the Near Boom results. For comparison, wind tunnel data recorded 0.15 m below and 0.9 m downstream of a scale model sprayer with a boom height of 0.65 m indicated a consistent upward *w* component between approximately 0.025 to 0.05 U_{ref} along most of the boom length (Teske et al., 2015). Scaling with the appropriate reference airspeeds from the present tests, the wind tunnel predicted *w* component values range between 0.18 and 0.43 m s^{-1} and between 0.43 and 0.77 m s^{-1} for eastbound and westbound reference airspeeds, respectively. The *w* component values below and behind the nozzles in figure 8 were upward and typically ranged from approximately 1.0 to 2.0 m s^{-1}. Considering the experimental sources of error present in both datasets, the relatively close agreement in the direction and relative magnitude of the upward components was encouraging. Aside from the variability expected in field tests, the boom of the wind tunnel model had only one structural member along its bottom chord, compared to the three structural tubes, hydraulic hose bundle, and wet boom tube that were located in the bottom half of the boom cross-section of the experimental sprayer. A greater blockage should be expected due to these elements, with the potential outcome of greater upwash downstream of the boom compared to the wind tunnel model.

The *w* component values were verified for normality, and a general linear model was fit based on speed, direction of travel, distance behind the nozzles, and lateral sensor position. A comparison of means is presented in table 10. Again, without normalizing by the reference airspeed, the significance of travel speed was expected; this highlights its impact as an operating choice. Across all treatments, the flow field had an average (downward) velocity component greater than 1.0 m s^{-1} immediately below the nozzles (position 3) and an upward mean velocity between 0.75 and 0.97 m s^{-1} in the other sensor positions.

Table 10. Comparison of mean *w* components of air velocity in the Far Boom region for the experimental treatments. Means with different letters under each treatment are significantly different according to Tukey's pairwise comparison tests at a 95% confidence level.

Treatment	Mean	Grouping
Travel speed (m s^{-1})		
4	0.277	a
11	0.808	b
Travel direction		
West	0.773	a
East	0.313	b
Lateral sensor location (m)		
8.30	0.511	ab
6.63	0.444	a
4.97	0.674	b
Position number		
1	0.791	a
2	0.854	a
3	-1.041	b
4	0.746	a
5	0.933	a
6	0.974	a

Behind Tractor

The mean direction of the vertical and lateral components of airflow measured in the Behind Tractor region are presented in figure 9, along with the average lateral component of ambient wind relative to the sprayer. For brevity, only data from measurements at 11 m s^{-1} are shown. Like the other locations, the trends were similar in the data measured at 4 m s^{-1}, but the component magnitudes were smaller. Westbound tests were into a headwind; eastbound tests were with the wind.

In figure 9, the arrows annotated with "-" indicate that any of the individual measurement runs contributing to the reported means had more than 2.5% of the anemometer elevation angle data outside of the elevation angle range and were recorded as extreme values of the elevation range

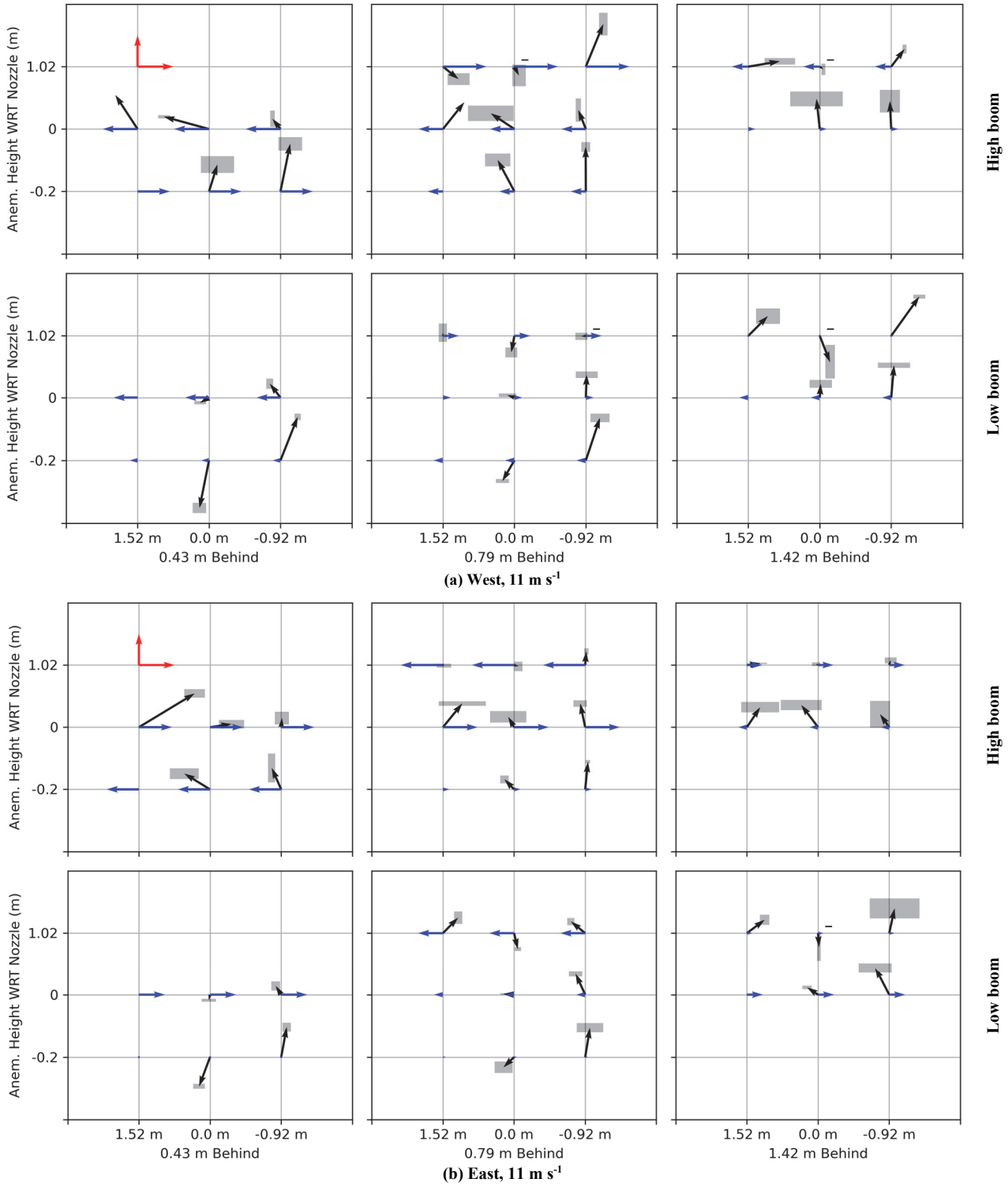

Figure 9. Multi-run average air velocity vectors (black arrows) measured in the Behind Tractor region in a plane normal to the direction of travel (*v*, *w*) at 11 m s^{-1} travel speed when traveling (a) west (headwind) and (b) east (tailwind). For each lettered set of plots, the high boom position (1.14 m; top) and low boom position (0.64 m; bottom) are shown.

(±60°). These vertically oriented vector quantities were typically associated with small airspeed magnitudes.

The *w* component values were divided into two categories (above the nozzles, and in the plane of and below the nozzles) in the same way as the streamwise velocity deficit values. The above-nozzle data were Johnson transformed (type SU) to achieve normality. General linear models were fit to both data subsets with factors for speed, direction, nozzle height, sensor location (height above and distance behind nozzles), and the lateral sensor position across the width of the machine. The fit of both models was poor ($R^2 < 0.5$ for both subsets), indicating that the significant scatter in the data could not be accounted for by the factors included in the

model. Therefore, only the following, limited, qualitative interpretations were possible.

At 11 m s^{-1} (east and west) and 4 m s^{-1} (east, not shown), the direction of the vertical component of flow reversed with the changes in boom height (centerline sensor, 0.2 m below, and 0.43 m behind). A lower operating height resulted in downward air velocity at this measurement location. It is suspected that this was due to interaction with the airflow under the tractor. Upward flow was observed at the sprayer centerline in the available wind tunnel data (Teske et al., 2015).

In contrast, the sensor at -0.92 m had a consistent upward direction of flow at nearly all measurement locations in the nozzle plane and below the nozzles. Additionally, the lower boom configuration tended to have larger upward velocities at the sensors with lateral position of 1.52 and -0.92 m when positioned 1.02 m above and 1.42 m behind the nozzles. On the centerline of the sprayer, measurements above the nozzles in the lower boom position at 11 m s^{-1} had a consistent downward component; this was attributed to downward flowing in-fill in the wake behind the tank. Because the location of the anemometer changed with the height of the boom, it was difficult to attribute the lack of this downward flow component at the higher boom position to a change in wake structure as opposed to measurement at a different elevation relative to the tank.

The dataset from the sensor laterally located at 1.52 m was incomplete due to the corruption of some measurement positions by dusty conditions (15 of 56); however, the direction of flow was also upward at many of the measurement locations (34 of 41 locations with reported values), even though this sensor was located farther from the centerline of the machine. Overall, this indicated a complex flow field behind the sprayer tractor, which was a likely result of the large blockage created by the tractor, airflow beneath and around the tractor, the moveable blockage presented by the boom, and the airflow patterns around the rotating tires.

TURBULENCE

The TKE of the measured air velocity is presented for data collected in the Far Boom and Behind Tractor regions. The sampling rate from the Near Boom dataset (4 Hz) was deemed too low compared to the two other regions (measured at 32 Hz) to capture velocity fluctuations with certainty.

Far Boom

The TKE data for the Far Boom region at travel speeds of 4 and 11 m s^{-1} are shown in figure 10. The magnitude of TKE was greater in the nozzle plane than 0.2 m below the nozzles. A speed sensitivity in both directions was noted in the horizontal plane through the nozzles; below the nozzles, TKE was effectively insensitive to the reference airspeed.

Given its outsized magnitude relative to the average values, the magnitude of TKE at the sensor in the nozzle plane laterally located 8.30 m and 0.79 m behind the nozzles was verified in the time data of the contributing runs. A notable increase in TKE was also measured downstream and only above the articulation points of the boom in wind tunnel sprayer tests (Teske et al., 2015). The normalized TKE values reported by Landry and Wolf (2019) when measured in

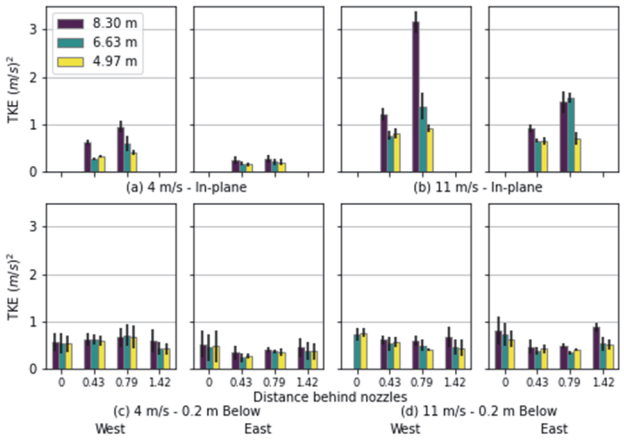

Figure 10. Mean TKE measured in the Far Boom region at travel speeds of (a and c) 4 m s^{-1} and (b and d) 11 m s^{-1} in the nozzle plane (a and b) and 0.2 m below the nozzles (c and d) while traveling west (headwind) and east (tailwind). Error bars represent standard deviations of the runs included in the mean.

the nozzle plane 3.69 m outside of the rear tires of a John Deere R4045 sprayer were approximately one order of magnitude greater compared to the values reported at a lateral position of 4.97 m in figure 10, after normalizing by $(U_{ref})^2$. However, the proximity to the boom structural elements was different between the two data sets, and the CFD results from that same work indicated a notable contribution to local turbulence patterns from the boom structural elements.

After applying a Johnson transformation (type SU) to the measured TKE data, a general linear model was fit with factors for travel speed, travel direction, lateral sensor position, and the measurement location behind and below the nozzles (see table 1 for sensor positions relative to the nozzle). All factors were found to be significant; a comparison of means is presented in table 11. However, the overall model fit was poor, with R^2 (adjusted) of 46.2%. A Tukey pairwise comparison computed a unique group for the mean of the sensor laterally located at 8.68 m, while the means of the other two lateral sensor locations were not significantly different from each other.

Table 11. Comparison of mean TKE values in the Far Boom region after Johnson transformation for the experimental treatments. Means with different letters under each treatment are significantly different according to Tukey's pairwise comparison tests at a 95% confidence level.

Treatment	Mean-Johnson	Grouping
Travel speed (m s^{-1})		
4	-0.463	a
11	0.501	b
Travel direction		
West	0.353	a
East	-0.315	b
Lateral sensor location (m)		
8.30	0.401	a
6.63	-0.118	b
4.97	-0.227	b
Position number		
1	-0.149	ab
2	0.541	c
3	0.281	bc
4	-0.262	a
5	-0.166	a
6	-0.132	ab

Elevated turbulence was measured at the farthest outboard sensor location (8.30 m); the anemometer position is shown in figure 11. Significant mechanical elements were present on the boom upstream of the sensor, including the hydraulic actuator for the outer boom section and additional boom structural elements. It was presumed that the measured increase in turbulence at this position was due to these additional bluff bodies present upstream of the sensor. Similar disturbances were observed at boom articulation points by Teske et al. (2016b). This highlights the potential effect that component packaging and placement can have on the airflow near the boom. Generalizing the structural blockage effects observed by Murphy et al. (2000) suggests an increased average elevation of the drift plume downstream of larger blockages.

Behind Tractor

The TKE data for the Behind Tractor measurement region at travel speeds of 4 and 11 m s^{-1} are shown in figure 12. Overall, the turbulence behind the tractor was greater than in the Far Boom region; in particular, greater TKE was observed at the two off-centerline positions compared to along the central plane of the tractor in the nozzle plane and below the nozzles. When normalized by $(U_{ref})^2$, the values measured at 11 m s^{-1} directly behind the tire in the nozzle plane (boom height = 1.14 m) ranged from 0.0167 to 0.021 (m s^{-1})^2. This agreed well with the reported range of 0.014 to 0.026 (m s^{-1})^2 measured by Landry and Wolf (2019) directly behind the rear tire of a John Deere R4045 sprayer. However, the CFD results from the same study indicated sharp local gradients in TKE behind the tire, so caution is needed in comparing the different datasets.

Similar to the analysis of the velocity deficit data measured in the same region, the dataset was split into two subsets: measurements at 1.02 m above the nozzles, and measurements in the nozzle plane and 0.2 m below the nozzles. To further identify factors that contributed to TKE, the normality of the subsets was verified, and a general linear model was developed using speed, direction, nozzle height, lateral sensor location, and the position of sensor relative to the nozzle (see table 1 for sensor positions relative to the nozzle). A Johnson transformation (type SB) was applied to the data above the nozzles, but normality requirements were met for the dataset in the nozzle plane and below the nozzles. A comparison of the means from both subsets is presented in table 12.

As expected, TKE increased with travel speed and the presence of a headwind. In both subsets, TKE was significantly lower at the sensor laterally located at 0.0 m compared to the other two locations. Nozzle height was a significant factor in the TKE in both subsets, but with opposite effects: a lower boom height correlated to a reduction in measured turbulence in the nozzle plane and below the nozzles but correlated with increased TKE 1.02 m above the nozzles. Overall, measured TKE was greater in the nozzle plane and below the nozzles compared to 1.02 m above the nozzles.

Figure 11. Position of ultrasonic anemometer laterally located at 8.30 m in the Far Boom measurement region. The anemometer is shown while measuring below the nozzle plane.

Conclusions and Future Work

Airflow measurements around a modern high-clearance sprayer were recorded during field operation for the purpose

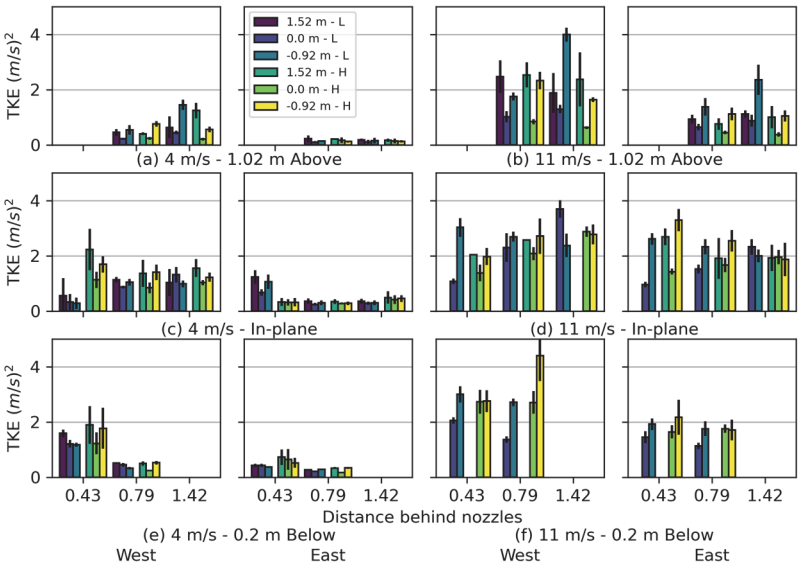

Figure 12. Mean TKE in the Behind Tractor region when traveling west (headwind) and east (tailwind) at travel speeds of (a, c, e) 4 m s^{-1} and (b, d, f) 11 m s^{-1} measured 1.02 m above the nozzles, in the nozzle plane, and 0.2 m below the nozzles at three lateral positions (1.52, 0.0, and -.92 m) and two boom heights (L = 0.64 m, H = 1.14 m). Error bars represent standard deviations of the runs included in the mean.

Table 12. Comparison of mean TKE values 1.02 m above the nozzles and in the nozzle plane and 0.2 m below the nozzles in the Behind Tractor region. Means with different letters under each treatment are significantly different according to Tukey's pairwise comparison tests at a 95% confidence level.

	1.02 m Above Nozzles		In Plane and 0.2 m Below Nozzles	
Treatment	Mean-Johnson	Grouping	Mean	Grouping
Travel speed (m s^{-1})				
4	-0.678	a	0.740	a
11	0.710	b	2.275	b
Travel direction				
West	0.457	a	1.817	a
East	-0.425	b	1.199	b
Lateral sensor location (m)				
1.52	0.192	a	1.626	a
0.0	-0.445	b	1.263	b
-0.92	0.300	a	1.635	a
Position number				
1	-0.062	a	-	
2	0.094	b	-	
3	-		1.492	a
4	-		1.481	ab
5	-		1.635	a
6	-		1.665	a
7	-		1.266	b
Boom height (m)				
0.64	0.109	a	1.419	a
1.14	-0.077	b	1.597	b

of better understanding how the wake was influenced by operating parameters and for validating future numerical simulations. The ultimate goal of this research is to understand and reduce the machine-induced flow conditions that increase the risk of pesticide drift.

Measurements were made in three different regions of the wake behind the sprayer along the boom: far out from the tractor (Far Boom), behind and outside of the rear tire of the tractor (Near Boom), and immediately behind the tractor (Behind Tractor). Three ultrasonic anemometers were used in each region.

Distinct regions were evident in the wake behind the sprayer. In the Far Boom region, airflow was seemingly uninfluenced by the sprayer tractor. The wake present immediately outboard of and behind the rear tire was complex. A large zone of stagnant air was present above the nozzles behind the tractor. Flow near and below the nozzles behind the tractor was also complex due to interactions with the underside of the tractor, the tires, and the blockage created by the boom support structure itself.

Several flow features that could potentially promote drift were identified:

- Flow behind and outside the rear tire was complex in the horizontal plane of the nozzles. A significant velocity reduction was measured behind the rear tire. The air velocity outside the tires was near the reference airspeed despite structural elements being present upstream. In the Far Boom region, these elements created a measurable velocity reduction. A potential cause of the minimal velocity deficit near the tractor is a local increase in the velocity of the flow passing outside of the tires. This could be due to momentum transfer from the tires themselves and flow acceleration under the sprayer tractor and potentially between the front and rear tires.
- In the Far Boom region, acceleration of air was measured immediately below the nozzles. While not unexpected (due to the blockage of the boom itself), this indicated that spray droplets would be injected into a region of higher-than-nominal airspeed, which may be detrimental. A velocity deficit existed downstream of the nozzles in their horizontal plane.
- The largest velocity deficit was present behind the tractor above the nozzles. Flow reversal was measured during some test runs along the centerline of the machine. However, this was not consistent through the lateral positions measured across the width of the tractor, indicating that large streamwise velocity gradients were present in the region. Large spatial gradients behind the tractor were measured in wind tunnel tests (Teske et al., 2015).
- In the Behind Tractor region, a velocity deficit existed in the nozzle plane and below the nozzles despite a suspected acceleration of flow under the sprayer tractor. The deficit was smallest at the center of the boom section behind the tractor.
- An upward component of velocity was consistently measured across nearly all sensor positions in the nozzle plane and below the nozzles. An exception to this was the downward component measured directly below the nozzles. On the centerline of the sprayer, reducing the boom height resulted in a change from an upward to a downward velocity component, suggesting a complex interaction with the airflow passing under the sprayer tractor.
- Flow patterns above the nozzles potentially indicated a recirculation zone behind the sprayer tank. While out of the direct path of droplets, droplets could become entrained in this region and thus be at a greater risk of drift in the presence of a crosswind.
- TKE was greater behind the tractor compared to the Far Boom region. This included in the nozzle plane and below the nozzles, which suggested that the flow field in proximity to droplet injection was more turbulent behind the sprayer tractor. Behind the tractor, TKE was greater near the tire compared to the centerline of the machine. Although Landry and Wolf (2019) did not compare TKE measurements across the wake behind the tractor, the complexity of flow and resulting turbulence near the rear tires was pronounced.
- In the Far Boom region, increased TKE was measured downstream of the boom articulation point and hydraulic actuator in some test conditions, similar to Teske et al. (2015). This suggested that the presence of bluff body objects as part of the boom can influence turbulence downstream and increase drift accordingly.

While only one model of sprayer was tested, it is likely that many of these detrimental features are present in the wakes of most current sprayers. This highlights opportunities both for more streamlined designs of the sprayer tractor

and boom structure in the future and for reducing the influence of operating choices on the aerodynamics of current sprayer designs through improved understanding. Nearly all the detrimental patterns noted were more severe with higher reference airspeed. This highlighted the benefit of reduced travel speeds as well as the contribution of the ambient wind in influencing the size of the sprayer wake. If spraying a field using a headwind and tailwind orientation, we would expect to see an increasing effect from the direction of travel on deposition variation with greater windspeeds. Future work to expand the test matrix used herein to include significant crosswind contributions would enable a more complete comparison of the effect of ambient wind on wake characteristics. A lower boom height improved the airflow conditions at the measurement locations immediately behind the sprayer to a limited degree. Operating with a lower boom height provides the additional benefit of reducing the trajectory length of droplets across the entire width of the sprayer. Considering the documented flow complexity related to the structure and tires at the rear of machine, more investigation via physical tests or CFD is warranted; the effects of tire rotation should be present in future efforts.

While the characteristics of the sprayer wake are important to understand, the trajectories of the spray droplets are the ultimate description of near-field pesticide drift. The cost and repeatability challenges of physical pesticide drift trials, in addition to field measurements like those in this study, suggests that validated multiphase CFD simulations, despite their computational cost and complexity, could be a more cost-effective and repeatable approach to predicting near-field drift across multiple operating scenarios.

Acknowledgements

The authors gratefully acknowledge the financial support of Alberta Pulse Growers, Manitoba Crop Alliance, Manitoba Pulse and Soybean Growers, Saskatchewan Pulse Growers, and the Western Grains Research Foundation, with support from Agriculture and Agri-Food Canada and the Canadian Agricultural Partnership. The authors also acknowledge Cervus Equipment and their John Deere Saskatoon dealership for making available the sprayer and test track. Finally, the authors acknowledge that this research was completed on Treaty 6 Territory and the Homeland of the Métis.

Reference to any specific commercial products by trade name, trademark, manufacturer, or otherwise, does not constitute or imply its endorsement or recommendation by the authors, their affiliated organizations, or the funders of this research.

References

Butler Ellis, M. C., & Miller, P. C. (2010). The Silsoe spray drift model: A model of spray drift for the assessment of non-target exposures to pesticides. *Biosyst. Eng., 107*(3), 169-177. https://doi.org/10.1016/j.biosystemseng.2010.09.003

Chou, Y., Polansky, A. M., & Mason, R. L. (1998). Transforming nonnormal data to normality in statistical process control. *J. Qual. Tech., 30*, 133-141. https://doi.org/10.1080/00224065.1998.11979832

Environment Canada. (2019). Historical data: Past weather and climate. Toronto, ON, Canada: Environment Canada. Retrieved from https://climate.weather.gc.ca/historical_data/search_historic_data_e.html

Landry, H., & Wolf, T. M. (2019). An investigation of airflow patterns created by high-clearance sprayers during field operations. *Canadian Biosyst. Eng., 61*, 2.01-2.12. https://doi.org/10.7451/CBE.2019.61.2.01

Minitab. (2019). Minitab 18. State College, PA: Minitab LLC.

Murphy, S. D., Miller, P. C., & Parkin, C. S. (2000). The effect of boom section and nozzle configuration on the risk of spray drift. *J. Agric. Eng. Res., 75*(2), 127-137. https://doi.org/10.1006/jaer.1999.0491

Nuyttens, D., De Schampheliere, M., Baetens, K., & Sonck, B. (2007). The influence of operator-controlled variables on spray drift from field crop sprayers. *Trans. ASABE, 50*(4), 1129-1140. https://doi.org/10.13031/2013.23622

Python. (2021). Python language reference. Fredericksburg, VA: Python Software Foundation. Retrieved from https://docs.python.org/3/reference/

Teske, M. E., Bird, S. L., Esterley, D. M., Curbishley, T. B., Ray, S. L., & Perry, S. G. (2002). AgDrift: A model for estimating near-field spray drift from aerial applications. *Environ. Toxicol. Chem., 21*(3), 659-671. https://doi.org/10.1002/etc.5620210327

Teske, M. E., Thistle, H. W., Lawton, T. C., & Petersen, R. L. (2016a). Evaluation of the flow downwind of an agricultural ground sprayer boom. *Trans. ASABE, 59*(3), 839-846. https://doi.org/10.13031/trans.59.11442

Teske, M. E., Thistle, H. W., Petersen, R. L., Lawton, T. C., Guerra, S. A., & Funseth, T. G. (2015). Evaluation of the wake of an agricultural ground sprayer. *Trans. ASABE, 58*(3), 621-628. https://doi.org/10.13031/trans.58.10996

Teske, M. E., Thistle, H. W., Petersen, R. L., Lawton, T. C., Guerra, S. A., & Funseth, T. G. (2016b). Evaluation of the wake of an agricultural ground sprayer with the wind from any direction. *Trans. ASABE, 59*(5), 1205-1219. https://doi.org/10.13031/trans.59.11844